Journal of Colloid and Interface Science 725 (2027) 141313

Contents lists available at ScienceDirect

Journal of Colloid And Interface Science

journal homepage: www.elsevier.com/locate/jcis

Structured emulsions in switchable soft-matter for formulating stable pharmaceutical microcrystal suspensions

Purnima N. Manghnani [f], Ariel Yi Hui Chua [f], Serene Ming En Chong [g], Arif Z. Nelson [g], Saif A. Khan [d,e,*], Patrick S. Doyle [a,b,c,**]

[a] Singapore-MIT Alliance for Research and Technology, 1 CREATE Way, #04-13/14 Enterprise Wing, 138602, Singapore
[b] Department of Chemical Engineering, Massachusetts Institute of Technology, 77 Massachusetts Avenue Room E17-504F, Cambridge, MA 02139, USA
[c] Harvard Medical School Initiative for RNA Medicine, Boston, MA 02115, USA
[d] Department of Chemical and Biomolecular Engineering, National University of Singapore, 4 Engineering Drive 4, Singapore 117585, Singapore
[e] Singapore-MIT Alliance for Research and Technology, 1 CREATE Way, #04-13/14 Enterprise Wing, 138602, Singapore
[f] Singapore-MIT Alliance for Research and Technology, 1 CREATE Way, #04-13/14 Enterprise Wing, 138602, Singapore
[g] Food, Chemical and Biotechnology Cluster, Singapore Institute of Technology, 1 Punggol Coast Road, 828608, Singapore

HIGHLIGHTS

- Structured emulsions template monodisperse sub-10 μm API crystals.
- pH-switchable Carbopol enables droplet generation, stability and confinement.
- Bottom-up approach yields narrow, uniform particle size distributions.
- Monodispersity of bottom-up suspensions suppresses Ostwald ripening.
- Redispersible composite films recover crystals without size distribution loss.

GRAPHICAL ABSTRACT

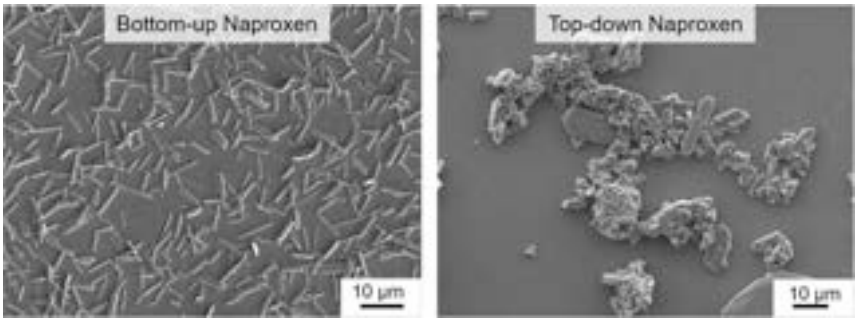

ARTICLE INFO

Keywords:
Microcrystals
Structured emulsions
Stable suspensions
Yield-stress

ABSTRACT

Long-acting drug delivery systems depend on crystalline suspensions with tightly controlled particle size to ensure reliable delivery and long-term stability, yet producing sub-10 μm crystals with narrow and persistent size distributions remains challenging. Here we introduce a bottom-up crystallization strategy in which monodisperse, pH-switchable structured emulsions act as transient microreactors that template active pharmaceutical ingredient microcrystals during anti-solvent crystallization. Confinement of droplets within a yield-stress soft-matter matrix enables the formation of highly uniform naproxen microcrystals (~7 μm). In contrast to conventional wet-bead milling, the resulting suspensions exhibit substantially reduced Ostwald ripening under accelerated stability conditions while preserving crystal form and injectability-relevant size. The method is readily scalable via membrane emulsification and supports downstream solid dosage formats, demonstrated by

* Corresponding author at: Department of Chemical and Biomolecular Engineering, National University of Singapore, 4 Engineering Drive 4, Singapore 117585, Singapore.
** Corresponding author at: Singapore-MIT Alliance for Research and Technology, 1 CREATE Way, #04-13/14 Enterprise Wing, 138602, Singapore.
E-mail addresses: saifkhan@nus.edu.sg (S.A. Khan), pdoyle@mit.edu (P.S. Doyle).

https://doi.org/10.1016/j.jcis.2026.141313
Received 4 May 2026; Received in revised form 15 July 2026; Accepted 4 August 2026
Available online 8 August 2026

redispersible thin films. Together, this work establishes structured emulsions as a generalizable platform for engineering stable, monodisperse crystalline suspensions for long-acting drug delivery.

1. Introduction

Chronic diseases often require frequent drug administration, contributing to treatment burden, pill fatigue, and poor patient adherence. Long-acting drug delivery systems offer an attractive strategy to extend drug exposure and reduce dosing frequency by controlling the rate at which an active pharmaceutical ingredient (API) is released over time. Across long-acting formulations, the physicochemical and structural attributes of the drug particles including particle size, size distribution, crystal form, and surface properties play a central role in governing dissolution, physical stability, and ultimately drug-release kinetics [1,2]. Particle engineering is therefore a critical component in the development of long-acting drug products, particularly for poorly water-soluble small molecules (BCS Class II and Class IV) for which crystalline particles can themselves serve as sustained drug reservoirs. Developing scalable strategies to precisely engineer and preserve these crystalline particle attributes in suspension form remains a key challenge in achieving robust and reproducible long-acting drug delivery.

Crystalline pharmaceutical suspensions typically contain API crystals in an aqueous medium comprising excipients such as wetting agents, flocculants, buffers, and viscosity modifiers. The size of the API crystals largely influences the performance of these suspensions, as it governs both drug dissolution kinetics and injectability. To achieve sustained release, microcrystals are preferred over nanocrystals, since nanocrystals can dissolve faster, leading to a burst release. Furthermore, for the suspension to be injectable, the upper size limit is 20 μm. Most intramuscularly administered aqueous suspensions on the market have a particle size of 1–10 μm [1]. Another important formulation feature is the particle size distribution of the crystalline API. A large particle size distribution may lead to an unpredictable dissolution rate, and the suspension may be prone to Ostwald ripening, an undesirable formulation outcome. Ostwald ripening occurs when large API crystals grow at the expense of smaller crystals [3]. This happens due to the higher surface energy of small crystals leading to their dissolution, often facilitated by the presence of surfactants and/or organic solvents. It is, therefore, desirable to have a narrow size distribution.

Generally, crystalline API suspensions are produced using top-down techniques, such as wet-media milling, high-pressure homogenization, or jet milling, where large crystals obtained via conventional crystallization processes are broken down into smaller crystals through impact and shear forces. These techniques are well understood and widely applied but have some inherent drawbacks. Milling can lead to API amorphization [4], polydisperse particle outcomes [5], polymorphic transition [6], surface fractures [7,8], and chemical degradation [9]. The process also influences particle stability – for example, agglomeration resulting from particle-particle collisions, the development of electrostatic charge, or the long-term stability of initially stable crystalline surfaces under mechanical strain [10]. The stability of top-down suspensions is strongly influenced by the choice of polymers or surfactants that decorate the particle surface. These surface modifiers are essential for achieving particle breakdown (sub-20 μm) but can interact with the API in the resulting suspension, leading to crystal growth. This is notable for lipophilic APIs with a relatively high water solubility. Alternative bottom-up approaches, such as anti-solvent crystallization or spray-drying, involve building crystals from a molecular state. While these approaches have been shown to provide a better handle on particle size and crystallinity, they generally have low yields due to difficulties in accurately controlling supersaturation [3,11].

Simultaneous and facile control over particle size, solid state, stability, and performance is extremely challenging, considering the sensitivity of the crystallization process to different process parameters for different APIs. Crystallization of APIs in emulsion droplets has shown significant promise in addressing these particle engineering challenges [12–14]. Oil-in-water emulsion droplets in the 5–50 μm size range can serve as individual small batch reactors for the isolation of the precipitation process and formation of micro-crystals in the 1–10 μm size range. Conventionally, emulsions in the 10–500 μm size range are produced using rotor-stator systems, high-pressure homogenizers, or ultrasound-assisted techniques. These generally require high energy input and lead to polydisperse emulsions and particles. In this aspect, microfluidic droplet generation has been successfully applied to generate monodisperse emulsions in the 100–500 μm size range for API crystallization [15,16]. While microfluidics offers superior precision, for emulsions in the 5–50 μm range, it inherently has a low production yield, high susceptibility to clogging and wetting problems, and complex scale-up process. In this regard, membrane emulsification offers several distinct advantages over microfluidic droplet generation, particularly regarding production scale and system simplicity. High-throughput fabrication of monodisperse emulsions in the 5–50 μm range has been achieved through membrane emulsification and has been applied for the fabrication of microparticles [17–19]. The pre-mix operation mode of membrane emulsification is a low-energy process that involves the disruption of the dispersed phase droplets in a coarse emulsion through a microporous membrane made of glass or stainless steel. Both droplet sizes and size distributions can be tuned simply by changing the membrane pore size and the number of passages [20].

Another concern with emulsions in the micrometer size range is that they are prone to density-driven separation. In the absence of continuous agitation, these emulsions exhibit creaming or sedimentation [12]. Continuous agitation, however, can lead to unwanted droplet breakup and emulsion non-homogeneity. In the absence of back-to-back droplet generation and precipitation, as is anticipated for a batch process, a lag between the two can lead to emulsion destabilization. In a new approach called embedded droplet printing, oil droplets were generated and manipulated in an aqueous yield-stress fluid for pharmaceutical crystallization [13,21]. Through the structured nature of the semi-solid fluid having a yield stress, the droplets were held in place, isolated from the neighboring droplets. This process led to the formation of highly monodisperse particles in the hundreds of micrometers size range.

Here, a monodisperse emulsion of ethyl acetate (EA) containing a model BCS Class II drug, Naproxen (NPX), was produced through membrane emulsification in a structure-switchable aqueous phase, followed by anti-solvent crystallization to generate monodisperse NPX micro-crystals. More specifically, an oil-in-water emulsion of NPX was formed in an aqueous phase containing Carbopol (CP), where the CP performed two functions: first, at low pH, it acted as a tensioactive agent during the membrane emulsification to facilitate droplet breakup, and second, it switched into a structured fluid at high pH to prevent emulsion separation. The emulsion droplets were then subjected to solvent extraction in an anti-solvent under sonication, leading to NPX crystallization. The NPX micro-crystals were characterized using static light scattering (SLS), powder X-ray diffraction (PXRD), differential scanning calorimetry (DSC), Fourier-transform infrared spectroscopy (FTIR), optical microscopy, and electron microscopy to validate their solid-state outcome and morphology. Furthermore, we conducted an accelerated stability study to compare the ripening propensity of bottom-up NPX microcrystals with those obtained through conventional milling methods under compositionally matched conditions. While prior studies have explored the fabrication of 1–10 μm microcrystals through typical anti-solvent crystallization, this work is the first to combine microfluidic-like precision with the scalability of membrane emulsification to fabricate microcrystals in the sub-10 μm size range. This can

serve as a generalizable platform for engineering stable, monodisperse crystalline suspensions for long-acting drug delivery. The NPX micro-crystals obtained through the above approach were also formulated into a solid dosage form, reconstitutable thin films, with the promise of predictable particle size distribution and, therefore, performance.

2. Experimental section

2.1. Materials

Naproxen (≥98.5%), Felodipine (≥99%), Artemether (≥98%) were purchased from Chemigran Pte. Ltd. Polyvinylpyrrolidone (PVP K30), Poly(D,L-lactide-*co*-glycolide) (PLGA 50:50, MW 30–60 kDa), Pluronic F-127 (PF127), sodium alginate (Sigma 71,238), ethyl acetate (anhydrous, 99.8%), pyrene, polyacrylic acid (PAA, MW 130 kDa), and sodium hydroxide were purchased from Merck, Singapore. SPG membranes and membrane holders were purchased from SPG Technology Co., Ltd. The membranes used in this study were hydrophilic membranes of 50 μm pore size. The membranes were used without any further modification. Carbopol 980NF (cross-linked polyacrylic acid particles) was purchased from Lubrizol. Ethanol (≥99.8%) and acetone (≥99.8%) were purchased from VWR Singapore. All chemicals were used as received. Cell strainers with a mesh size of 40 μm were purchased from Fisher Scientific. Ultrapure water (18.2 MΩ) was obtained from a Sartorius H_2OPRO-DI-T Arium Pro purifier.

2.2. Surface activity of Carbopol

0.2, 0.5, 1, and 2 wt% CP dispersions and PAA solutions (pH-unmodified) were prepared in DI water and drop-cast onto polyvinylidene fluoride (PVDF) membranes to measure the contact angle of the resulting droplet using an optical goniometer (OCA 15EC, DataPhysics Instruments GmbH). Pendant drop characterization was performed using the same optical goniometer. 4 μL of EA-saturated CP dispersions (0, 0.2, 0.4 wt%) were injected into a water-saturated EA reservoir. The drop contours were recorded, and interfacial tension between the two phases was estimated using the Young-Laplace equation [22].

Surface tension of CP was also characterized indirectly by using pyrene as a fluorescent molecular probe. Pyrene was added to Carbopol dispersions (0, 0.05, 0.1, 0.2, 0.4 wt%) at 1 μM concentration, and the samples were agitated in an orbital shaker at 200 RPM at room temperature for 24 h. Pyrene emission spectra were recorded from 350 to 500 nm in a Cary Eclipse Fluorescence Spectrometer, with the excitation at 336 nm and slit widths set to 5 and 10 for excitation and emission, respectively. The ratio of the intensity at the first (I_I at 373 nm) and the third (I_{III} at 383 nm) vibronic peaks was used as an index of local hydrophobicity of CP aggregates [23,24].

To probe the mechanical response of the droplet interface under compressive deformation, pendant-drop experiments were performed using a rapid step-retraction protocol. 1 μL of EA in 0.4% CP and 4 μL of 0.4% CP in EA pendant drops were first formed and allowed to extract and equilibrate for 1200 s and 600 s respectively, enabling the development of the interfacial layer. The drop volume was then rapidly reduced by withdrawing at 2 μL/s of the dispersed phase through the needle, imposing a sudden decrease in interfacial area and, consequently, a compressive stress at the interface.

2.3. Rheological characterization of structured emulsions

Neat emulsions were prepared with neat ethyl acetate as the dispersed phase. An aqueous solution of 0.2 wt% CP (pH 3.5) saturated with ethyl acetate served as the continuous phase. The emulsion composition was maintained at 90% (*v*/v) continuous phase and 10% (v/v) dispersed phase (DP). A coarse emulsion was generated by gently manually agitating the two phases and then loading them into 50 mL syringes for the membrane emulsification process. The emulsion was passed back and forth across a 50 μm pore size membrane for a total of 25 cycles using programmed syringe pumps operating at 120 mL/min (Video S1). 1 M Sodium hydroxide was added to the emulsion to adjust its pH to approximately 4.1 and 5.2. Dynamic viscoelastic and viscosity measurements of the emulsions at different pH levels were performed by a Discovery HR30 Rheometer (TA Instruments). For the flow sweep test, rotational steady shear was performed with a tool geometry of a concentric cylinder to measure the flow behavior of the emulsions and the viscosity as a function of the shear rate, increasing from 1 to 100 s^{-1}. The Herschel-Bulkley model was fitted to the flow sweep curves to obtain the yield stress of the emulsions.

2.4. Characterization of emulsion droplet size

We characterized the emulsion droplet size using three different strategies:

a. Through templating PLGA: PLGA was dissolved in ethyl acetate at a concentration of 100 mg/mL. The emulsion composition and membrane emulsification procedure were maintained as stated for the neat emulsions in the previous section. For the stirred batch of emulsions, we stirred the coarse emulsion for 30 min on a stir plate at 800 RPM. After the emulsion was structured at pH 5.2, it was added to a water bath as the precipitating anti-solvent sink. PLGA was templated onto the emulsion droplets to yield PLGA microspheres.
b. Through optical imaging of the emulsion sandwiched between glass slides. We observe droplet evaporation at the periphery of the glass slides and therefore, acquire images quickly at the center of the sample before any droplet movement ensues.
c. Through static light scattering of the neat emulsion (no active in dispersed phase) diluted in a bath that is pre-saturated with ethyl acetate. This ensures that the droplets do not extract immediately upon dilution and maintain their size. Albeit dynamic due to ethyl acetate volatility, this is a more direct read of the droplet size and provides the necessary quantitative analysis.

2.5. Production of NPX micro-crystals

NPX was dissolved in ethyl acetate at a concentration of 50 mg/mL. The emulsion composition and emulsification procedure were maintained as stated for the neat emulsions in the previous section. After the emulsion was structured at pH 5.2, it was added to ultrapure water under probe sonication at 20 W for 15 s (Qsonica Sonicator Q500). The NPX formed micro-crystals upon extraction of the ethyl acetate emulsion droplets in water and were subsequently held in a glass petri dish overnight to evaporate the ethyl acetate. The suspension was then treated with 1 M NaOH until the suspension pH was ~ 6.5. PVP was added to the NPX suspension to obtain a concentration of 0.02 wt%. The crystals were harvested using centrifugation and diluted with PVP and PF127 to obtain a final suspension concentration of 0.5 wt% NPX in 0.02 wt% PF127 and 0.02 wt% PVP.

2.6. Top-down NPX micro-crystals

0.25 g of NPX in 20 mL of 0.05 wt% PF127 was wet-bead milled for 30 min at 500 RPM in a PM 100 Retsch ball mill with 2 mm ZrO_2 balls. The final suspension was adjusted to 0.5 wt% NPX in 0.02 wt% PF127 and 0.02 wt% PVP to maintain formulation parity between the bottom-up and top-down approaches.

2.7. Particle characterization

NPX micro-crystal size distributions were characterized through static light scattering (Malvern Mastersizer 3000E) and polarized light microscopy (PLM). During light scattering measurements, if the NPX

suspension contained PF 127, 1 mL of the suspension was added to 200 mL of water saturated with NPX and 0.02 wt% PF127 and sonicated for 180 s before size measurement. All the sizing statistics were obtained over 10 consecutive static light scattering runs. The images obtained through PLM were analyzed using an image-based segmentation algorithm to determine the length and width of the microcrystals accurately [25]. NPX micro-crystal morphology was examined using field emission scanning electron microscopy (FESEM, 7610, JEOL). Before FESEM observation at an operating voltage of 5 kV, dried samples were sputter-coated with a layer of platinum. The polymorphism of crystalline NPX was characterized by powder X-ray diffraction (PXRD), which ranged from a 2θ angle of 4° to 40° at a scan rate of 1° min^{-1}. The solid-state properties of the NPX crystals were characterized through a DSC thermogram obtained using DSC25 with Tzero pans from TA Instruments. Each sample was heated from −10 to 125 °C at a rate of 10 °C min^{-1}. The micro-crystals were further analyzed using Fourier transform infrared spectroscopy (Bruker Tensor 27). Finally, the NPX mass loading (*w/v*) in the suspensions was determined using a Cary 60 UV–visible spectrophotometer. Approximately 500 μL of the suspension was placed in 500 μL of ethanol and allowed to dissolve for 2 h. The NPX load was determined by comparing the measured UV–visible spectrum peak at 331 nm to a calibration curve obtained in the concentration range of 6.5 to 52 μg/mL NPX dissolved in a 50% ethanol-water solution.

2.8. Accelerated stability study

The suspensions generated through top-down and bottom-up approaches were cycled between 40 °C for 7 h and −20 °C for 17 h. The suspensions were drawn at days 3 and 7 for particle size characterization.

2.9. Solid composite forms

The NPX suspensions were formulated into solid composite forms to prototype possible product outcomes for redispersion at the point of use. For fabricating a redispersible thin film, sodium alginate was added to the primary suspension such that the final concentration was 1% NPX, 0.02% PVP, and 1.5% sodium alginate. This solution was cast onto a hydrophobic glass template and dried in the oven at 70 °C to obtain an NPX thin film. We re-dispersed the film in water to recover the NPX micro-crystals and characterized their size distribution.

3. Results

3.1. Generating structured monodisperse emulsions

To fabricate monodisperse sub-10 μm API crystals, we must first create monodisperse dispersed phase (DP) droplets (10–30 μm) that can template the crystals. Emulsions within this size range are readily produced using membrane emulsification. In the next step, the emulsion must be structured to prevent density-driven droplet segregation and coalescence until anti-solvent precipitation is performed (Fig. 1a). With this rationale, Carbopol (CP), a cross-linked particulate form of polyelectrolyte polyacrylic acid (PAA), was identified as a surface-active structure-setting polymer that could provide both low interfacial tension at low pH and a transition to a yield-stress fluid at high pH (Fig. S1). First, a premixed emulsion of active-laden ethyl acetate (EA) in 0.2 wt% dispersion of CP (pH unmodified) was passed back and forth through a 50 μm SPG membrane with programmed syringe pumps (Fig. 1a and b). The emulsion pH at this stage was ~ 3.5, allowing the tensioactive CP to enable maximum droplet breakup. The emulsion was collected and structured by adjusting the pH of the emulsion to ~ 5.2. The emulsion was then added to an anti-solvent sink under sonication to induce precipitation of the active. Due to the volatility of EA, the emulsion was characterized for its size distribution through three methods. First PLGA, a model polymer that templates into spherical particles, was used as an active surrogate in the dispersed phase. Upon extraction, we obtained PLGA microparticles that exhibited a monodisperse particle size distribution, in contrast to those generated through stirring (Fig. 1c). A theoretical droplet diameter of the emulsion was estimated by performing a simple mass balance calculation with the PLGA particle D_{50} as 4.4 μm. The calculated droplet diameter was ~ 10 μm (Section S2). Second, through optical imaging of the neat emulsion sandwiched between two glass slides, we obtained an average size of ~11 μm. Third, through static light scattering of the neat emulsion diluted in an aqueous bath pre-saturated with EA, a D_{50} of 13.4 μm was obtained (Figs. S2 c and d).

3.2. Carbopol duality aids structured emulsion generation

The surface activity of the monomer of CP, polyelectrolyte PAA, has been widely studied [26]. The surface activity of CP, however, has not been explored in the context of emulsion generation. Here, we

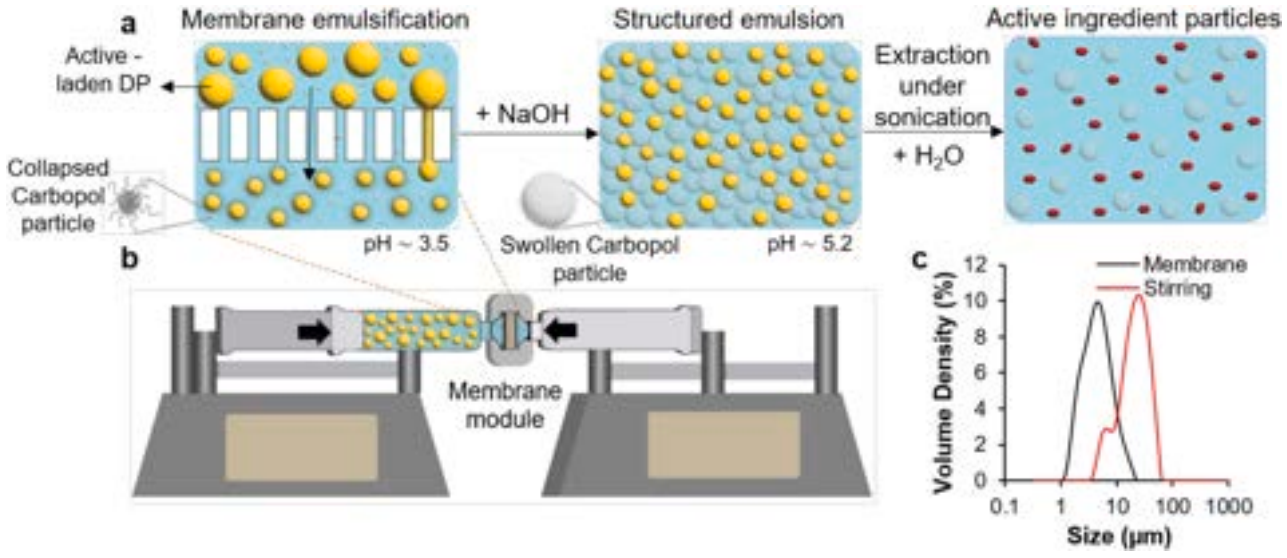

Fig. 1. a. Schematic representing the process of emulsion generation, structuring and anti-solvent extraction to template active ingredient particles. **b.** Automated membrane emulsification performed through programmed syringe pumps pushing the coarse emulsion back and forth for droplet breakup. **c.** Static light scattering size distributions of templated PLGA particles obtained through membrane emulsification and stirring emulsification.

characterized the surface activity of CP, first, by casting droplets of CP dispersions (pH-unmodified) onto hydrophobic PVDF membranes and measuring the contact angle with an optical goniometer. As seen in Fig. 2a, 1 % CP showed a visible reduction in contact angle in comparison to DI water, indicative of its surface activity. In comparison to a 2% PAA solution, the 2% CP dispersion showed a moderate reduction in contact angle as seen in Fig. S3. This was attributed to the development of weak yield stress at higher CP concentrations [27,28]. To further probe the tensioactivity of CP, we performed a pendant drop analysis of EA-saturated CP dispersions in water-saturated EA. In Fig. S4, the pendant drop contours of 0, 0.2 and 0.4 wt% CP are shown. Using the shape factor obtained through the droplet aspect ratio method [22], we estimated the interfacial tension by solving the Young-Laplace equation (Section S3). A decreased interfacial tension of 0.2 wt% CP (7.85 mN/m) and 0.4 wt% CP (7.72 mN/m) was obtained in comparison to DI water (10.28 mN/m). However, we suspect that the weak yield stress of CP dispersions could affect the droplet dynamics, preventing the actual presentation of its tensioactivity. Therefore, we tested the improvement in local hydrophobicity through the solubilization of a hydrophobic fluorescent probe in the CP dispersion. A highly sensitive test is the measurement of the change in emission spectrum of pyrene with respect to the polymer composition in an aqueous solution [23]. The fluorescence spectra of pyrene in water in the presence of CP are shown in Fig. S5. A characteristic increase in the emission intensity of pyrene with an increase in CP concentration was recorded. Furthermore, in the presence of CP, the vibronic band III of pyrene increases due to its incorporation in the hydrophobic domains of the polymer chain and therefore, leads to a decrease in the intensity ratio of emission peaks at 373 nm and 383 nm (I_I/I_{III}). The decrease in the I_I/I_{III} for the aqueous CP dispersions in Fig. 2b shows that pyrene is increasingly protected from the aqueous environment with higher CP content. An illustration for the CP particle assembly on the oil-water interface was proposed in Fig. 2c, where, similar to that suggested for PAA assembly at the oil-water interface [29], at low pH, the polymer trains adsorb to the interface with the protonated carboxylic groups oriented away from the interface. CP, similar to PAA, loses its surface activity, leading to emulsion phase separation at higher pH due to the deprotonation and relaxation of the polymer chains (Fig. S6). To further probe interfacial complexity, equilibrated pendant drops of EA in CP solution and vice versa were subjected to rapid volume reduction to impose a sudden compressive deformation at the interface (Fig. S7) [30]. Post equilibration and extraction, EA droplets in a 0.4% CP reservoir, as would be the case in our emulsion, retracted smoothly, indicating a fluid-like interface. However, 0.4% CP in an EA reservoir showed pronounced buckling upon retraction, indicating a non-fluid-like interfacial response. This response suggests the formation of a mechanically arrested interface with solid-like character (See section S3).

The structure switch of the emulsion at high pH was examined and shown visually in Fig. 2d. At pH 3.5, post-emulsion generation, it exhibited a significant amount of creaming within 2 h. The behavior was markedly different at pH 5.2, where the CP underwent a degree of structuring to prevent buoyancy-driven droplet segregation. This observation was supported by the flow sweep tests of the emulsions shown in Fig. 2e. At pH 4.1 and 5.2, the emulsions had higher yield stress (σ_Y) values compared to the low pH emulsions. The emulsion droplets were therefore held in place due to the yield stress imparted by the swollen CP microgels and droplet interaction was inhibited due to the CP segments adsorbed onto the oil-water interface. The force exerted on the emulsion droplet due to the yield stress of the emulsion was compared to the force due to buoyancy from the density difference in Section S5 [21]. The yield-stress force on a single DP droplet was estimated to be significantly higher than the buoyancy force exerted by the droplet on

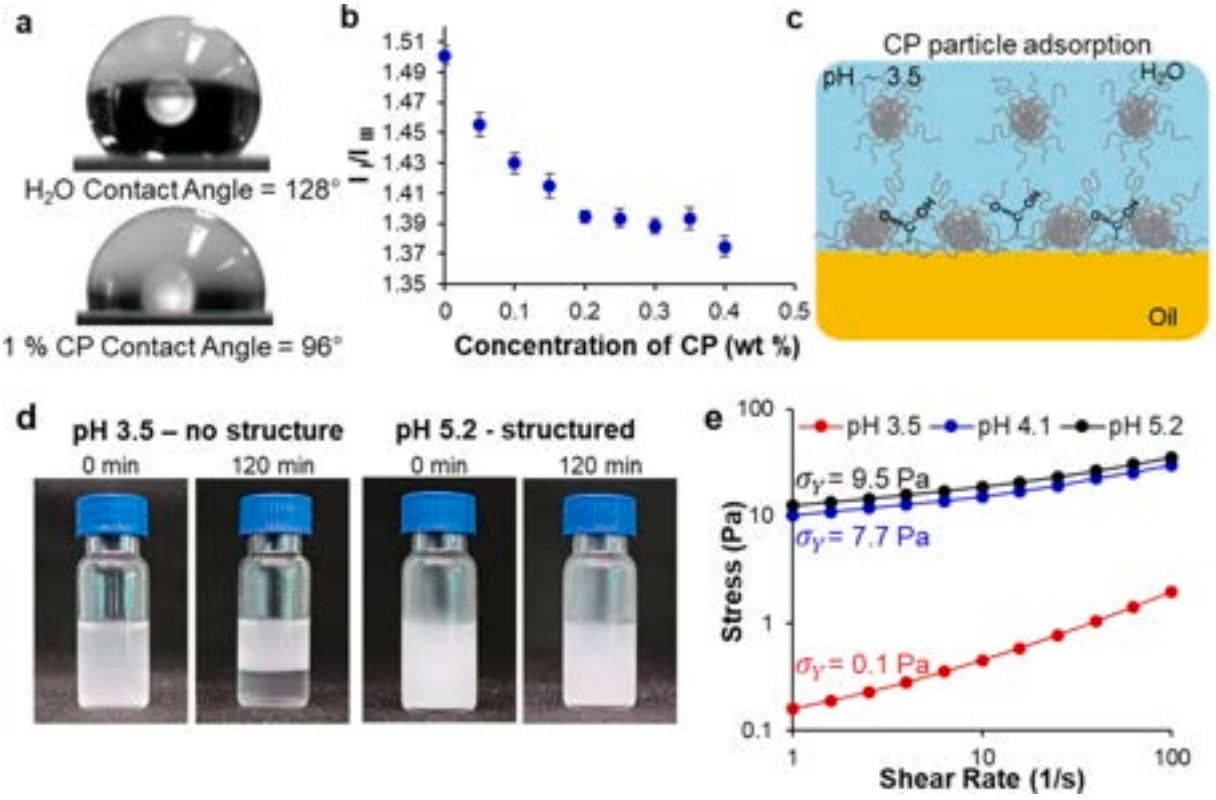

Fig. 2. **a.** Contact angle measurements of water and 1% Carbopol (CP) on a hydrophobic PVDF membrane. **b.** Ratio of the first to third vibronic peaks of pyrene as a function of CP concentration, **c.** Schematic depicting the adsorption of CP particles to the oil-water interface. **d.** Visual characterization of creaming propensity of ethyl acetate emulsions when the CP is not structured at pH 3.5 and is structured at pH 5.2. **e.** Flow behavior of the ethyl acetate-CP emulsions with different pH, the yield stress of the emulsion is indicated with the symbol σ_Y.

the bath.

3.3. Structured emulsion for bottom-up NPX micro-crystals

NPX-laden emulsions were generated through membrane emulsification and structure-set before anti-solvent extraction under sonication. Upon dilution in water, NPX crystallized and formed a dilute suspension of 0.05 wt% NPX. Post solvent evaporation, the suspensions were treated with PVP K30 to prevent the aggregation of the microcrystals [31], and the crystals were harvested using centrifugation. The resulting primary suspension had a composition of 0.5 wt% NPX and 0.02 wt% PVP. These bottom-up (BU) suspensions were characterized for their crystal size distribution using PLM and SLS techniques. The images of the NPX micro-crystals obtained using PLM showed remarkable uniformity (Fig. 3a). These micro-crystal populations were sized using edge-based detection algorithms [25] to obtain the length and width of the anisotropic crystals. The histograms in Fig. 3b and c show a mean length of 7.9 μm and a mean width of 2.9 μm. The microcrystals were also sized using SLS, as shown in Fig. 3d. The D_{50} of the BU NPX was 2.5 μm, which was distinct from the raw NPX powders with a D_{50} of 27.8 μm (Fig. S9). The anisotropic morphology of the BU NPX micro-crystals was confirmed through FESEM imaging in Fig. 3e. The crystallinity of the BU NPX micro-crystals was compared with raw NPX powder in Fig. 3f. The BU NPX displayed identical solid-state characteristics of the raw form. In Fig. 3g, the DSC curves for the BU NPX micro-crystals showed a single melting endotherm at 158.8 °C, similar to the melting point of raw NPX at 159.2 °C. This confirmed that the same polymorph of NPX was obtained through the emulsion templating approach. In Fig. 3h, the FTIR spectrum for the BU NPX micro-crystals showed the peaks of the raw NPX spectrum, devoid of any characteristic peaks of PVP or CP. This confirmed that the two excipients used did not change the NPX crystal form. Upon neutralization of CP and dilution for extraction, we expect it to be in its swollen, non-tensioactive state with density very close to water and therefore be separated out in the centrifugation and washing step. To confirm this, we visualized the primary suspension (no separation or washing) and the centrifuged suspension using optical microscopy. As shown in Fig. S10, the CP forms a marked film like residue if present in the suspension (~0.016%) and a washed suspension is devoid of any such residue. This indicates that we have negligible amount of CP in the final suspension. In contrast to CP, we expect PVP K30 molecules to decorate the NPX micro-crystal surface and impart it with re-suspendibility [31]. This was easily confirmed by evaluating the NPX suspensions with and without the addition of PVP as the stabilizer. As seen in Fig. S11, NPX suspensions with no PVP underwent severe and irreversible aggregation upon centrifugation evidenced by the SLS size characterization. Whereas NPX suspensions with 0.02% PVP did not aggregate and were easily re-suspendable. We assume that the PVP is fully adsorbed as a monolayer on the crystal surface.

As a proof of concept, this BU particle engineering approach was also applied for other model APIs, felodipine and artemether, and we successfully templated micro-crystals in a sub-10 μm domain shown in Fig. S12. In extending this approach to other APIs, we recognize that differences in molecular attributes and crystallization dynamics necessitate process adaptation. We therefore employ a decision framework based on two key API-specific attributes: (i) API solubility in the dispersed solvent phase, EA, and (ii) crystallization propensity, broadly categorized according to glass-forming behavior as fast-crystallizing (Class I) or slow-crystallizing (Classes II and III) molecules. These attributes guide the selection of the target emulsion droplet size and agitation conditions to achieve the desired particle-size distribution and crystalline solid-state outcome. The molecular structures and EA solubilities of representative model APIs are summarized in Fig. S13.

For example, felodipine exhibits substantially higher solubility in ethyl acetate than naproxen and is a relatively slow crystallizer. Because the droplets generated using our current emulsification method are approximately 10 μm in size and our target is the sub-10 μm crystal-size regime, further tailoring of the emulsion droplet size is not required for this API. However, felodipine forms an amorphous or oil-like intermediate prior to nucleation [32], requiring adaptation of the post-emulsification processing conditions. We find that mild agitation, rather than sonication, promotes more uniform nucleation for such slowly nucleating molecules. In contrast, artemether is a fast-nucleating

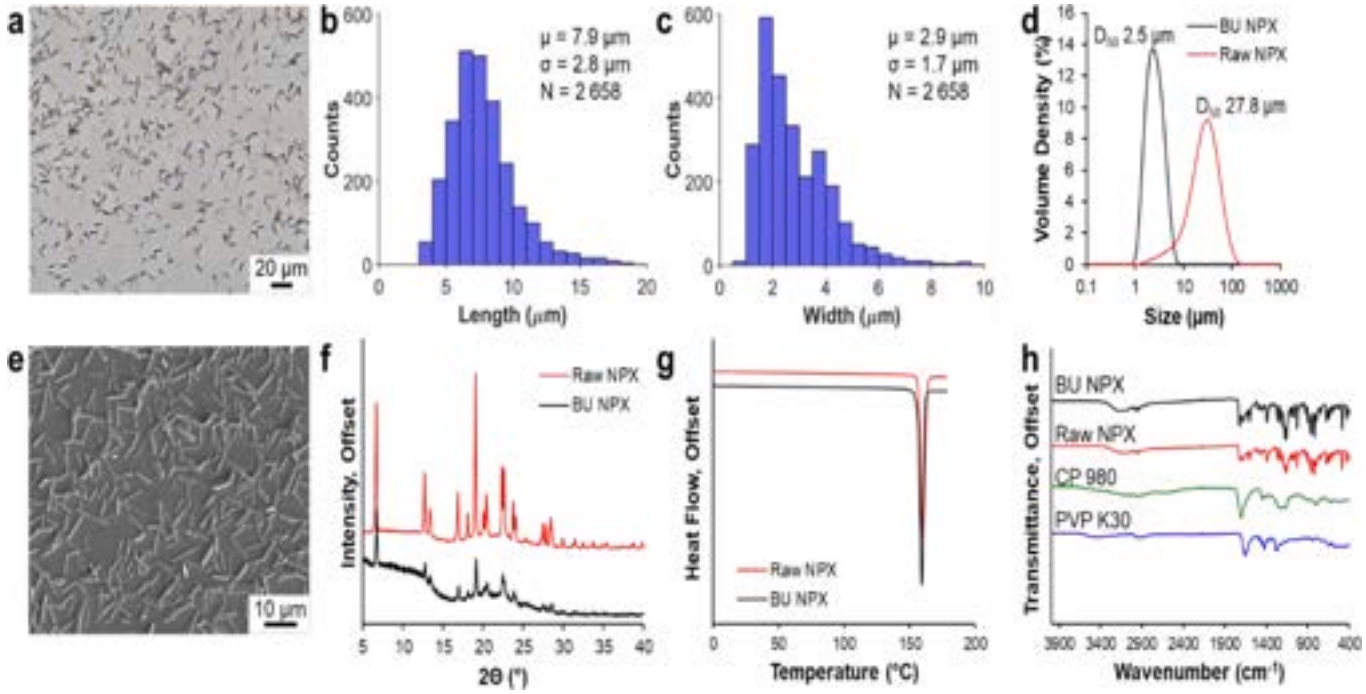

Fig. 3. a. Polarized light micrograph of the bottom-up (BU) NPX micro-crystals, **b, c.** Size distribution histograms obtained through image analysis of the PLM micrographs of the BU NPX crystals. **d.** Static light scattering size distributions of the BU and raw NPX crystals. **e.** FESEM micrograph of the BU NPX crystals. **f.** PXRD curves of the BU and raw NPX crystals **g.** DSC thermograms of BU and raw NPX crystals, and **h.** FTIR spectra of BU NPX, Raw NPX, CP 980 and PVP K30.

API with high solubility in the dispersed phase; consequently, the sonication step is retained to facilitate the formation of artemether microcrystals. Together, these observations highlight how API-specific solubility and crystallization kinetics can be used to rationally adapt the structured-emulsion process across chemically diverse molecules.

3.4. Bottom-up versus top-down: an accelerated stability study

An accelerated stability test for the BU NPX suspensions was performed and compared to suspensions generated through top-down wet-bead milling approach at the same excipient composition. This was aimed at studying the Ostwald ripening propensity of the crystal suspensions by subjecting them to elevated stress conditions. The top-down suspensions were generated through wet-bead milling of the raw NPX in a PF127 aqueous solution (D_{50} = 4.9 μm) shown in Fig. S14. The top-down and BU suspensions were adjusted in compositions such that the final composition for both were 0.5 wt% NPX, 0.02 wt% PVP and 0.02 wt% PF127. These suspensions were exposed to repeated freeze-thaw cycles between −20 °C and 40 °C for 7 days. The NPX suspensions were subjected to particle sizing using both SLS and PLM at different time points. In Fig. 4a, the evolution of the size distribution for top-down NPX crystals is shown. It is important to note that the top-down NPX crystals have a bi-modal size distribution with a significant sub-micron population on day 0. This population disappears in the subsequent SLS curve on day 3, and the D_{50} shifts to 9.44 μm with a significant increase in the span. Day 7 shows a dramatic shift in the particle size curve with an increase in the D_{50} to 22.1 μm indicating the ripening of larger crystals at the expense of small ones. The PLM characterization in Fig. 4b and c also indicates a shift in the size distribution of the top-down NPX crystals with time. A definitive increase in both average size and span was observed and depicted in the size distribution histograms. When particles are subjected to mechanical fracture during milling, the particle size distribution outcome is of prime importance. However, the changes in the particle surface properties are also being recognized as consequence that can lead to downstream issues. According to the attachment energy model, crystal fracture most likely occurs along the slip plane with the lowest attachment energy which leads to crystal surfaces with high propensity for growth [33]. Therefore, in addition to polydisperse particle size distribution, milling also leads to crystals with problematic surfaces and particle shapes [34].

In contrast to the top-down crystal ripening, the BU NPX microcrystals showed a monodisperse particle outcome on each day of characterization. The SLS curves obtained on days 3 and 7 were identical to that of day 0 in Fig. 4d. Furthermore, the optical micrographs seen in Fig. 4e and f corroborate that the crystal size distributions do not change drastically over the seven days. This suggests that under compositionally matched conditions, the BU NPX micro-crystals do not ripen in the same manner as top-down crystals. By ensuring monodispersity, the BU process suppresses long-term microcrystal ripening. Additionally, we suspect it minimizes crystal-facet heterogeneity, yielding more predictable particle outcomes.

3.5. Dispersible solid composites

In addition to the suspension form of the API, it can be formulated into solid forms depending on the end application. One such dosage form was prototyped using sodium alginate as a redispersible excipient. For a redispersible thin film, the BU NPX micro-crystals were simply mixed with sodium alginate to obtain final suspensions of 1% NPX, 0.02% PVP, and 1.5% sodium alginate. Taking advantage of sodium alginate's film-forming property, the above suspension was cast onto a hydrophobic glass template and dried at 70 °C to obtain a thin film

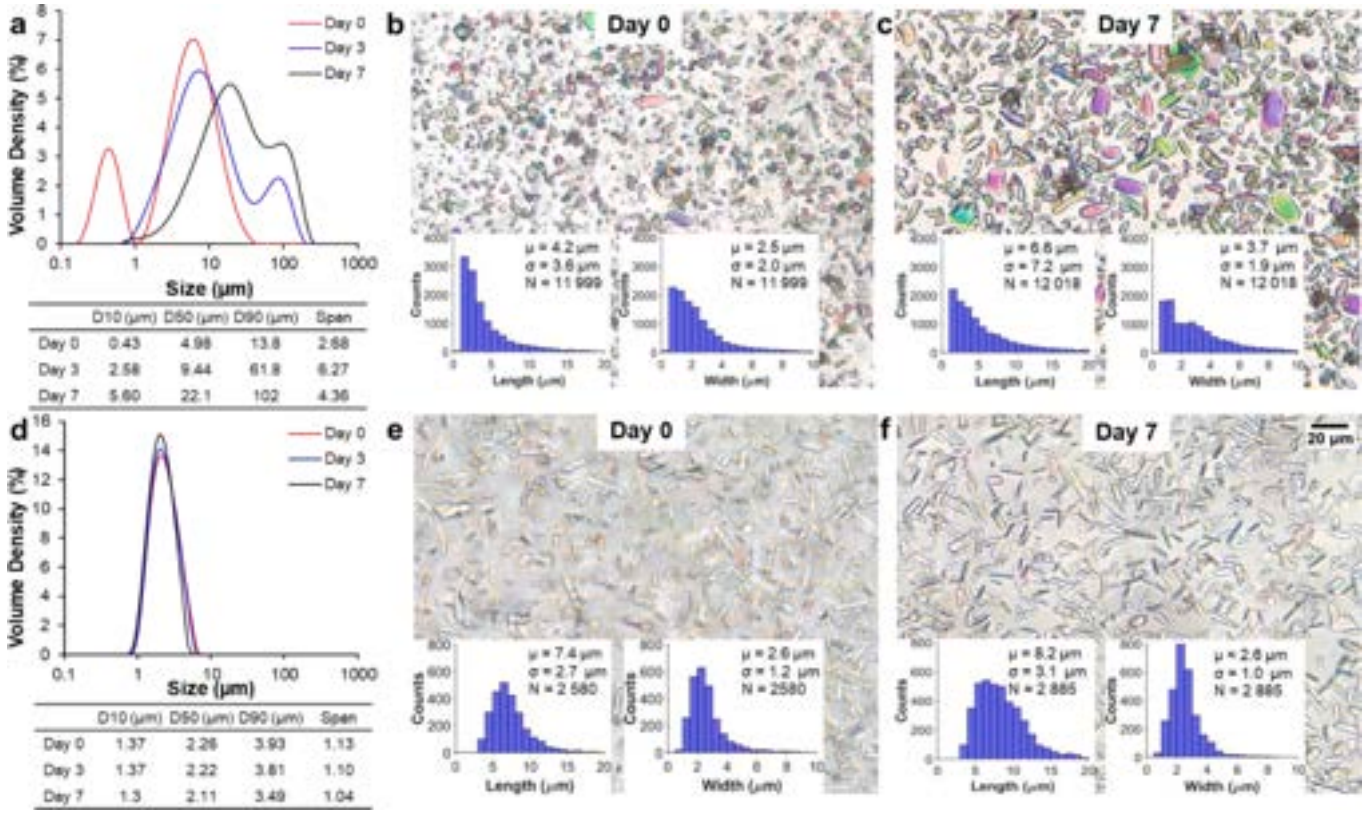

Fig. 4. a. Static light scattering size distributions of the top-down NPX crystals over 7 days of accelerated stability testing. **b, c.** Optical micrographs and their respective size distribution histograms obtained through image analysis of the PLM micrographs for the top-down NPX crystals. **d.** Static light scattering size distributions of the BU NPX crystals over 7 days of accelerated stability testing. **e, f.** Optical micrographs and their respective size distribution histograms obtained through image analysis of the PLM micrographs for the BU NPX micro-crystals.

composite shown in Fig. 5a. This film was readily reconstituted in DI water to obtain the embedded NPX micro-crystals with the original size distribution, as evidenced in Fig. 5b and c.

4. Conclusion

Predictable performance of long-acting pharmaceutical formulations hinges on controllable particle size distributions in the sub-10 μm size range. In this regard, monodisperse emulsion droplets in sizes less than 50 μm can act as transient microreactors to physically confine crystal growth of APIs, enabling precise control over particle size and producing highly uniform microcrystals that are difficult to achieve through kinetic control alone. To template these emulsions, however, comes with inherent stability challenges. In this work, we addressed these challenges by generating highly monodisperse and structured active-laden oil-in-water emulsions of 10 μm droplet size. While the monodispersity ensured particle size restriction, the structure prevented emulsion droplet interaction allowing for the generation of a crystalline API suspension with a tight size distribution in the sub-10 μm size range. We leveraged the switchability of Carbopol in terms of its surface activity and yield stress to produce structured emulsions, where the oil droplets were spatially trapped until they were solidified through anti-solvent extraction.

Current bottom-up particle engineering approaches face a fundamental trade-off between the precision of microfluidic crystallization [15,16] and the scalability of bulk anti-solvent processes [3], while established top-down methods such as wet milling [9,34] can introduce crystal defects and promote Ostwald ripening. Confined and emulsion-based crystallization strategies have improved particle-size control, but maintaining monodispersity, suspension stability, and manufacturable throughput simultaneously remains challenging. This work advances the field by coupling physical confinement in monodisperse microreactors with membrane-emulsification scalability, effectively bridging microfluidic-like particle precision and bulk production. Importantly, the enhanced resistance to Ostwald ripening suggests that the advance extends beyond initial particle-size control to preservation of the engineered size distribution during storage - a critical unmet need for long-acting injectable suspensions.

Naproxen suspensions formulated through this approach showed remarkable particle uniformity and stability in comparison to polydisperse top-down suspensions generated through wet-media milling. The suspensions were easily formulated into a solid dosage form that could be reconstituted to recover the original API crystals. The next major step will be demonstrating the process at pilot and commercial scale. If the reported performance persists, this approach could occupy an attractive niche between conventional anti-solvent crystallization (highly scalable but variable) and microfluidic crystallization (highly precise but low throughput). We envision a new manufacturing paradigm in which crystal size and stability are engineered by design rather than corrected by milling, potentially enabling more predictable and longer-lasting injectable medicines.

CRediT authorship contribution statement

Purnima N. Manghnani: Writing – original draft, Methodology, Formal analysis, Data curation, Conceptualization. **Ariel Yi Hui Chua:** Formal analysis, Data curation. **Serene Ming En Chong:** Formal analysis, Data curation. **Arif Z. Nelson:** Supervision, Methodology, Funding acquisition, Conceptualization. **Saif A. Khan:** Writing – review & editing, Supervision, Funding acquisition, Conceptualization. **Patrick S. Doyle:** Writing – review & editing, Supervision, Funding acquisition, Conceptualization.

Declaration of competing interest

The authors declare that they have no known competing financial interests or personal relationships that could have appeared to influence the work reported in this paper.

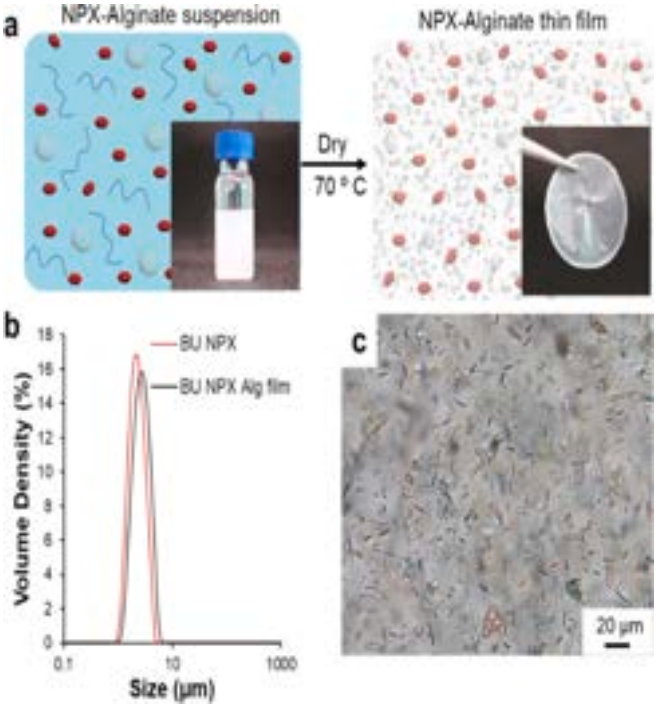

Fig. 5. a. Schematic demonstrating the casting and drying of an NPX-Alginate film, with an inset image of the film composite. **b.** Static light scattering size distributions of the bottom-up NPX crystals and the NPX crystals re-dispersed from the NPX-Alginate film. **c.** PLM images of NPX crystals re-dispersed from the NPX-Alginate film.

Acknowledgement

This research was supported by the Pharma Innovation Programme Singapore (grant number M23B3a0003). The authors thank Dr. Mei Lee and Dr. Stephanie Lam, GSK, Dr. John Hone, Syngenta, Luke Schenck, Merck and Dr. Pankaj Doshi, Pfizer for their valuable insight. The authors also thank Professor Sui Zhang for providing the optical goniometer for pendant drop analysis.

Appendix A. Supplementary data

Supplementary data to this article can be found online at https://doi.org/10.1016/j.jcis.2026.141313.

Data availability

No data was used for the research described in the article.

References

[1] V.T.T. Nguyen, N. Darville, A. Vermeulen, Pharmacokinetics of long-acting aqueous nano-/microsuspensions after intramuscular administration in different animal species and humans—a review, AAPS J. 25 (1) (2022) 4.
[2] K. Park, A. Otte, T. Li, Bohemian rhapsody of future drug delivery systems: rational changes necessary for the next revolution, Mol. Pharm. 21 (8) (2024) 3732–3742.
[3] A.A. Thorat, S.V. Dalvi, Liquid antisolvent precipitation and stabilization of nanoparticles of poorly water soluble drugs in aqueous suspensions: recent developments and future perspective, Chem. Eng. J. 181–182 (2012) 1–34.
[4] A.A. Elamin, C. Ahlneck, G. Alderborn, C. Nyström, Increased metastable solubility of milled griseofulvin, depending on the formation of a disordered surface structure, Int. J. Pharm. 111 (2) (1994) 159–170.
[5] F. Hládek, S. Chvíla, O. Navrátil, M. Balouch, F. Štěpánek, Systematic investigation of wet-milling kinetics and colloidal stability of pharmaceutical nanocrystals, Cryst. Growth Des. 22 (12) (2022) 6928–6940.

[6] A. Dupont, M. Guerain, F. Danède, L. Paccou, Y. Guinet, A. Hédoux, et al., Kinetics and mechanism of polymorphic transformation of sorbitol under mechanical milling, Int. J. Pharm. 590 (2020) 119902.
[7] J.C. Feeley, P. York, B.S. Sumby, H. Dicks, Determination of surface properties and flow characteristics of salbutamol sulphate, before and after micronisation, Int. J. Pharm. 172 (1) (1998) 89–96.
[8] T. Školáková, A. Kutějová, A. Školáková, P. Zámostný, The hidden impact of wet and dry milling processes on pharmaceutical surfaces, Int. J. Pharm. 681 (2025) 125870.
[9] S. Kumar, D.J. Burgess, Wet milling induced physical and chemical instabilities of naproxen nano-crystalline suspensions, Int. J. Pharm. 466 (1) (2014) 223–232.
[10] D.J. Am Ende, P.R. Rose, Strategies to achieve particle size of active pharmaceutical ingredients. Fundamentals of early clinical drug development, 2006, pp. 247–267.
[11] N. Rasenack, B.W. Müller, Micron-Size drug particles: common and novel micronization techniques, Pharm. Dev. Technol. 9 (1) (2004) 1–13.
[12] S. Kwon, K.M. Thomas, R. Lakerveld, Integrated membrane emulsification and solution cooling crystallization to obtain a narrow and predictable crystal size distribution, Chem. Eng. Process. Process Intensif. 171 (2022) 108751.
[13] A.Z. Nelson, B. Kundukad, W.K. Wong, S.A. Khan, P.S. Doyle, Embedded droplet printing in yield-stress fluids, Proc. Natl. Acad. Sci. 117 (11) (2020) 5671–5679.
[14] S. Shikha, Y.W. Lee, P.S. Doyle, S.A. Khan, Microfluidic particle engineering of hydrophobic drug with eudragit E100—bridging the amorphous and crystalline gap, Mol. Pharm. 19 (11) (2022) 4345–4356.
[15] R.A.L. Leon, A.Z.M. Badruddoza, L. Zheng, E.W.Q. Yeap, A.I. Toldy, K.Y. Wong, et al., Highly selective, kinetically driven polymorphic selection in microfluidic emulsion-based crystallization and formulation, Cryst. Growth Des. 15 (1) (2015) 212–218.
[16] E.W.Q. Yeap, D.Z.L. Ng, A. Prhashanna, A. Somasundar, A.J. Acevedo, Q. Xu, et al., Bottom-up structural design of crystalline drug-excipient composite microparticles via microfluidic droplet-based processing, Cryst. Growth Des. 17 (6) (2017) 3030–3039.
[17] A. Albisa, E. Piacentini, M. Arruebo, V. Sebastian, L. Giorno, Sustainable production of drug-loaded particles by membrane emulsification, ACS Sustain. Chem. Eng. 6 (5) (2018) 6663–6674.
[18] M.M. Dragosavac, G.T. Vladisavljević, R.G. Holdich, M.T. Stillwell, Production of porous silica microparticles by membrane emulsification, Langmuir 28 (1) (2012) 134–143.
[19] G.T. Vladisavljević, Structured microparticles with tailored properties produced by membrane emulsification, Adv. Colloid Interf. Sci. 225 (2015) 53–87.
[20] L. Giorno, G. De Luca, A. Figoli, E. Piacentini, E. Drioli, Membrane emulsification: principles and applications. membrane operations, 2009, pp. 463–497.
[21] A.Z. Nelson, J. Xie, S.A. Khan, P.S. Doyle, Continuous embedded droplet printing in yield-stress fluids for pharmaceutical drug particle synthesis, Adv. Mater. Technol. 6 (4) (2021) 2001245.
[22] F.K. Hansen, G. Rødsrud, Surface tension by pendant drop: I. A fast standard instrument using computer image analysis, J. Colloid Interface Sci. 141 (1) (1991) 1–9.
[23] V.A. De Oliveira, M.J. Tiera, M.G. Neumann, Interaction of cationic surfactants with acrylic acid−ethyl methacrylate copolymers, Langmuir 12 (3) (1996) 607–612.
[24] L. Piñeiro, M. Novo, W. Al-Soufi, Fluorescence emission of pyrene in surfactant solutions, Adv. Colloid Interf. Sci. 215 (2015) 1–12.
[25] A.Y.H. Chua, G.Y. Tan, E.W.Q. Yeap, D.M. Walker, J.M. Hawkins, S.A. Khan, Rapid, automated measurement of dynamic size distributions and size-dependent growth rates of crystal ensembles within microfluidic flow cells, Cryst. Growth Des. 22 (5) (2022) 2869–2879.
[26] B.N. Dickhaus, R. Priefer, Determination of polyelectrolyte pKa values using surface-to-air tension measurements, Colloids Surf. A Physicochem. Eng. Asp. 488 (2016) 15–19.
[27] I.A. Gutowski, The effects of pH and concentration on the rheology of Carbopol gels, 2010.
[28] Z. Jaworski, T. Spychaj, A. Story, G. Story, Carbomer microgels as model yield-stress fluids, Rev. Chem. Eng. 38 (7) (2022) 881–919.
[29] D.K. Beaman, E.J. Robertson, G.L. Richmond, Ordered polyelectrolyte assembly at the oil–water interface, Proc. Natl. Acad. Sci. 109 (9) (2012) 3226–3231.
[30] Y. Jiang, R. Chakroun, P. Gu, A.H. Gröschel, T.P. Russell, Soft polymer janus nanoparticles at liquid–liquid interfaces, Angew. Chem. 132 (31) (2020) 12851–12855.
[31] F. Anjum, M. Wessner, B. De Witte, N. Al-Rifai, A. Collas, G. Sadowski, Tailoring the use of excipients in bottom-up production of naproxen crystal suspensions via membrane technology, Int. J. Pharm. 652 (2024) 123846.
[32] H. Konno, T. Handa, D.E. Alonzo, L.S. Taylor, Effect of polymer type on the dissolution profile of amorphous solid dispersions containing felodipine, Eur. J. Pharm. Biopharm. 70 (2) (2008) 493–499.
[33] R. Ho, M. Naderi, J.Y.Y. Heng, D.R. Williams, F. Thielmann, P. Bouza, et al., Effect of milling on particle shape and surface energy heterogeneity of needle-shaped crystals, Pharm. Res. 29 (10) (2012) 2806–2816.
[34] J.Y.Y. Heng, F. Thielmann, D.R. Williams, The effects of milling on the surface properties of form i paracetamol crystals, Pharm. Res. 23 (8) (2006) 1918–1927.